Chemically induced partial unfolding of the multifunctional Apurinic/apyrimidinic endonuclease 1

Ratan Rai,[1] Olabode I. Dawodu,[1] Steven M. Johnson,[1] Jonah Z. Vilseck,[1,2,6] Mark R. Kelley,[1,3,4,5] Joshua J. Ziarek,[6] and Millie M. Georgiadis[1*]

[1] Department of Biochemistry and Molecular Biology, Indiana University School of Medicine, Indianapolis, IN 46202

[2]Center for Computational Biology and Bioinformatics, Indianapolis, IN 46202

[3]Herman B Wells Center for Pediatric Research, Department of Pediatrics, Indiana University School of Medicine, Indianapolis, IN 46202

[4]Department of Pharmacology and Toxicology, Indiana University School of Medicine, Indianapolis, Indiana 46202

[5]IU Simon Comprehensive Cancer Center, Indiana University School of Medicine, Indianapolis, IN 46202

[6]Department of Pharmacology, Northwestern University Feinberg School of Medicine, Chicago, Illinois, 60611.

[*]Corresponding author, Millie M Georgiadis, Email: mgeorgia@iu.edu

Abstract

Targeting of the multifunctional enzyme apurinic/apyrimidinic endonuclease I/redox factor 1 (APE1) has produced small molecule inhibitors of both its endonuclease and redox activities. While one of the small molecules, the redox inhibitor APX3330, completed a Phase I clinical trial for solid tumors and a Phase II clinical trial for Diabetic Retinopathy/Diabetic Macular Edema, the mechanism of action for this drug has yet to be fully understood. Here, we demonstrate through HSQC NMR studies that APX3330 induces chemical shift perturbations (CSPs) of both surface and internal residues in a concentration-dependent manner, with a cluster of surface residues defining a small pocket on the opposite face from the endonuclease active site of APE1. Furthermore, APX3330 induces partial unfolding of APE1 as evidenced by a time-dependent loss of chemical shifts for approximately 35% of the residues within APE1 in the HSQC NMR spectrum. Notably, regions that are partially unfolded include adjacent strands within one of two beta sheets that comprise the core of APE1. One of the strands comprises residues near the N-terminal region and a second strand is contributed by the C-terminal region of APE1, which serves as a mitochondrial targeting sequence. These terminal regions converge within the pocket defined by the CSPs. In the presence of a duplex DNA substrate mimic, removal of excess APX3330 resulted in refolding of APE1. Our results are consistent with a reversible mechanism of partial unfolding of APE1 induced by the small molecule inhibitor, APX3330, defining a novel mechanism of inhibition.

Introduction

The reliance of cancer cells on robust DNA repair has spurred the development of small molecule inhibitors targeting DNA repair proteins including the multifunctional apurinic/apyrimidinic endonuclease 1/redox effector factor 1 (referred to here as APE1).[1-2] APE1 is critical for the repair of damaged bases in the base excision repair pathway. Damage to nucleobases from oxidation, alkylation, and spontaneous nucleobase loss in cells is chronic and extensive with estimates of at least 10,000 events within the genome of each cell per day; thus, repair is critical for maintaining genomic stability.[3] APE1 is dually targeted; under normal conditions, it is primarily localized in the nucleus with small amounts seen in the cytoplasm and mitochondria,[4] but under oxidative stress, APE1 is relocalized from the nucleus to the cytoplasm and mitochondria.[5-6] In both the nucleus and mitochondria, APE1 functions as a endonuclease to repair damaged DNA. The nuclear localization sequence (NLS) is located on the unstructured N-terminus (1-20) of the protein[7] and the mitochondrial targeting sequence (MTS) on the structured C-terminus (289-318)[6]. Exposure of the MTS would necessarily require at least partial unfolding of the protein. Other nuclease functions attributed to APE1 include 3'-5' exonuclease, 3'-phosdiesterase, nucleotide incision repair activity[8-10] and repair of damaged RNA.[11-12]

As a redox factor, APE1 has been reported to reduce several transcription factors (TFs) including AP-1, HIF-1α, NF-kB, STAT3, and others that are critical for cell growth and survival.[13] The redox activity of APE1 was first identified in the search for the factor regulating the redox state of AP-1.[14] The proposed mechanism was a thiol-exchange mechanism involving Cys65 as the nucleophile in APE1, which reduced disulfide bonds in AP-1 that prevented it from binding to DNA.[15-16] Subsequently, APE1 was identified as the redox factor responsible for reducing several other transcription factors.[9-10, 13] Reduction of TFs is relevant for many diseases;

specifically, reduction of HIF-1α, NF-kB, and STAT3 impacts angiogenesis/inflammation associated with retinal vascular diseases.[17] Cys65 has also been implicated in mitochondrial trafficking.[18]

Knock-down of APE1 in a xenograft model resulted in reduced tumor growth[19] supporting development of small molecule inhibitors targeting this protein. Since knock-down results in loss of both endonuclease and redox functions, development of small molecule inhibitors targeting one or the other function of APE1 has been important in defining the roles of these functions in cancer[9] and more recently in vascular retinal diseases.[17, 20] The first small molecule, (2E)-2-[(4,5-dimethoxy-2-methyl-3,6-dioxo-1,4-cyclohexadien-1-yl)methylene]-undecanoic acid (E3330 or APX3330) (Fig. 1), targeting APE1 was identified in 2000 and found to inhibit the redox function of APE1.[21-22]

Two different mechanisms have been proposed. One group reported through NMR studies that APX3330 bound to the endonuclease active site of APE1 and inhibited endonuclease activity at concentrations exceeding 100 μM,[23] well above EC50 values reported for inhibition of redox activity (~10 μM).[24] Using an alternative approach of coupling of N-ethylmaleimide (NEM) fingerprinting and intact mass spectrometry, we reported a time-dependent labeling of buried Cys residues with NEM consistent with partial unfolding of APE1 in the presence of APX3330.[25] There are 7 Cys residues in APE1 and no disulfide bonds; the two solvent accessible Cys residues (99 and 138) were readily modified by NEM in the absence of APX3330. No covalent adducts between APX3330 were observed by intact mass spectrometry.[25] In the presence of APX3330, we suggested that once Cys residues 65, 93, 208, 296, and 310 (normally buried within the interior of fully folded APE1) were modified with NEM, it would not be possible for APE1 to fully refold. Thus, partially unfolded APE1 molecules were trapped

through NEM modification. While incubation of APX3330 resulted in a population of partially unfolded APE1 molecules in these studies,[25-26] the mechanism of partial unfolding has yet to be determined.

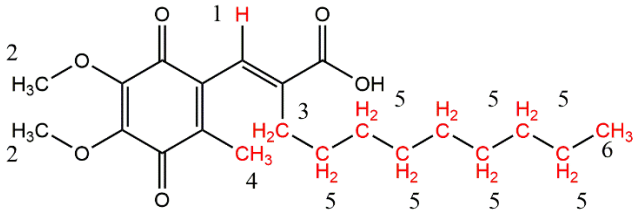

Fig. 1. Chemical structure of APX3330 (E3330). Protons with altered solvent accessibility in a 1D WaterLOGSY NMR experiment are highlighted in red. Numbers refer to assignments on the NMR spectra (SI Figure S6).

In the present study, we investigated the mechanism of action of APX3330 through HSQC NMR studies monitoring how its binding perturbs the native state of APE1. In a concentration- and time-dependent manner, APX3330 resulted in partial unfolding of APE1 involving three strands within one of the beta sheets and an adjacent alpha helix. Notably, the N-terminal strand involved in partial unfolding includes the redox critical residue Cys65. We further demonstrated that the partial unfolding is reversible upon removal of excess APX3330 in the presence of a substrate DNA mimic. These findings provide a basis for understanding subcellular trafficking of APE1 to the mitochondria and future drug development.

Results and Discussion

Increasing concentrations of APX3330 result in chemical shift perturbations of APE1

We assigned 234 backbone ^{1}H-^{15}N resonances, representing 90% of the possible 261 backbone resonances in the well-resolved HSQC spectra of ^{15}N-labelled APE1 (39-318/C138A), hereafter referred to as APE1, in buffer containing 20 mM sodium phosphate, 0.1 M sodium

chloride at pH 6.5 on a 600 MHz Bruker NMR spectrometer at 25 °C (SI Fig. S1) and demonstrated that the sample was stable for up to 20 days (SI Fig. S2). The assignments were made based on previously reported chemical shift assignments for APE1.[27] The C138A mutant was produced for crystallographic studies to avoid disulfide bond formation between Cys138 residue in two APE1 molecules in close proximity within the crystal lattice. We were unable to assign Ala138 since this differs in sequence from the reported work.[27] Equally well-resolved HSQC spectra were obtained at 30 °C and 35 °C (SI Fig. S3).

To examine interactions of the redox inhibitor APX3330 (Fig. 1) with APE1, we first identified a solvent that produced minimal chemical shift perturbations (CSPs). Two deuterated solvents were tested, DMSO and acetonitrile. Titration with DMSO alone produced significant CSPs (SI Fig. S4), while acetonitrile did not (SI Fig. S5). These results were consistent with crystallographic studies in which DMSO bound specifically to APE1,[28] thus all experiments were conducted using D3-acetonitrile to minimize solvent-mediated artifacts.

^{1}H-^{15}N HSQC spectra were acquired for a titration of APE1 with APX3330 at a 1, 2, 4, 6, 10, and 12-fold molar excess (Fig. 2). CSPs were assigned for the spectra with a 10-fold molar excess of APE1. The spectrum for the 12-fold molar excess was collected after 24 hours incubation and revealed a significant loss in the number of backbone resonances. The chemical shift perturbations for a 10-fold molar excess of APX3330 indicated a significant number of differences in backbone resonances spread throughout the protein. CSPs above a threshold of 0.02 include the following residues: Ile64, Ser66, Asp70, Arg136, Gln137, Ile146, Ser164, Ala175, Gly231, Ser252, Tyr264, Met271, Asn272, and Ser307 (Fig. 3a, b). Of these, 136, 137, and 164 are surface residues that define a small pocket on APE1, while 70, 271, and 272 border the endonuclease active site pocket on the opposite face of the protein (Fig. 3c, d). The only

other surface residues with significant CSPs are 146 and 307. The remaining residues with CSPs above 0.02 are located within the interior of the protein. Notably, residues 64 and 66 reside within a central strand in one of the two beta sheets that comprise the beta sandwich core of the protein, followed by a connecting loop that includes residue 70. Residues 271 and 272 reside within a loop adjacent to the endonuclease active site (Fig. 3e, f).

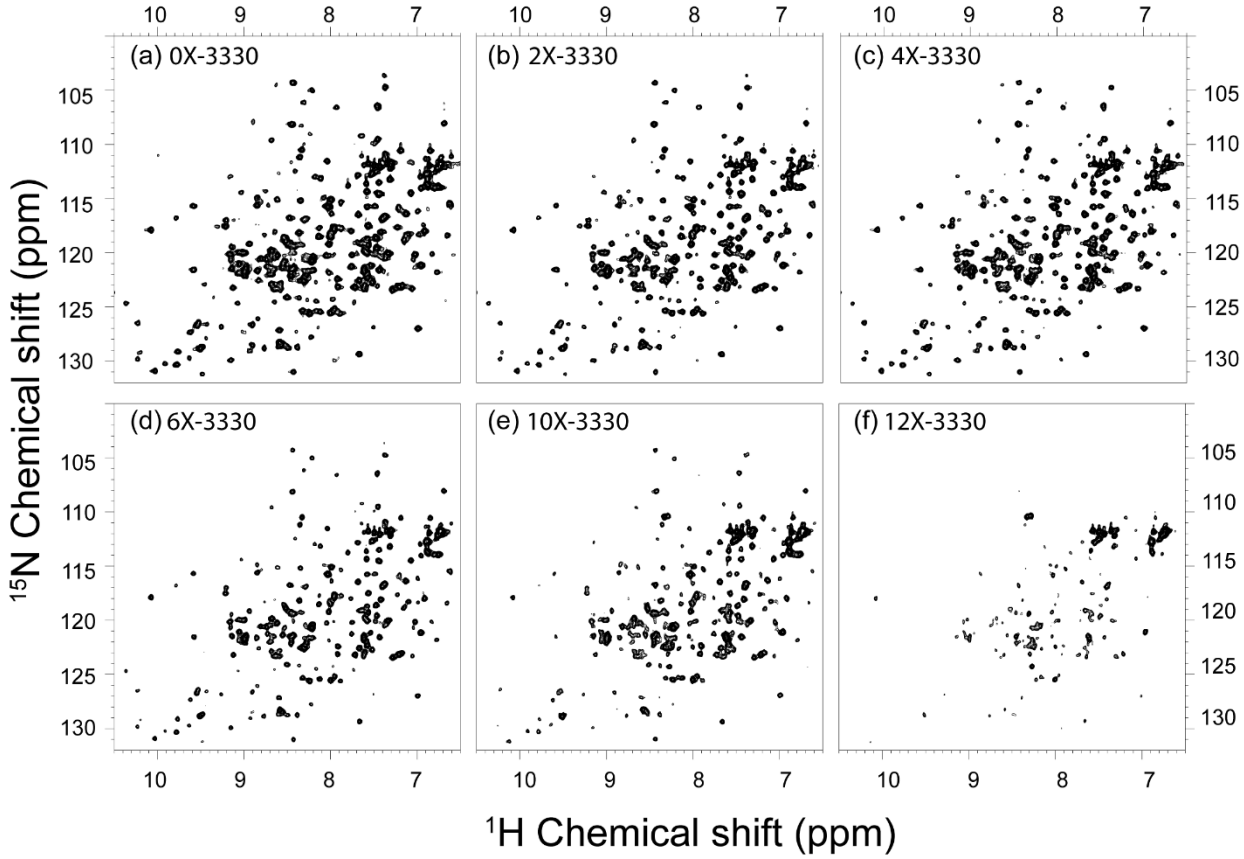

Fig. 2. Concentration dependent effects of APX3330 on [*U*-^{15}N]-APE1. All HSQC spectra were recorded on a single APE1 sample. (a) 2D HSQC spectra of (85 μM) free protein. Spectra with increasing APX3330 concentration (b) 2-fold APX3330 (c) 4-fold APX3330 (d) 6-fold APX3330 (e) 10-fold APX3330 and (f) 12-fold APX3330. It took a total of 24 hours to record all spectra. The time point for APX3330 titration is as follows (b) 2.0 h (c) 4.2 h (d) 6.3 h (e) 8.3 h (f) 24 h at 25 °C.

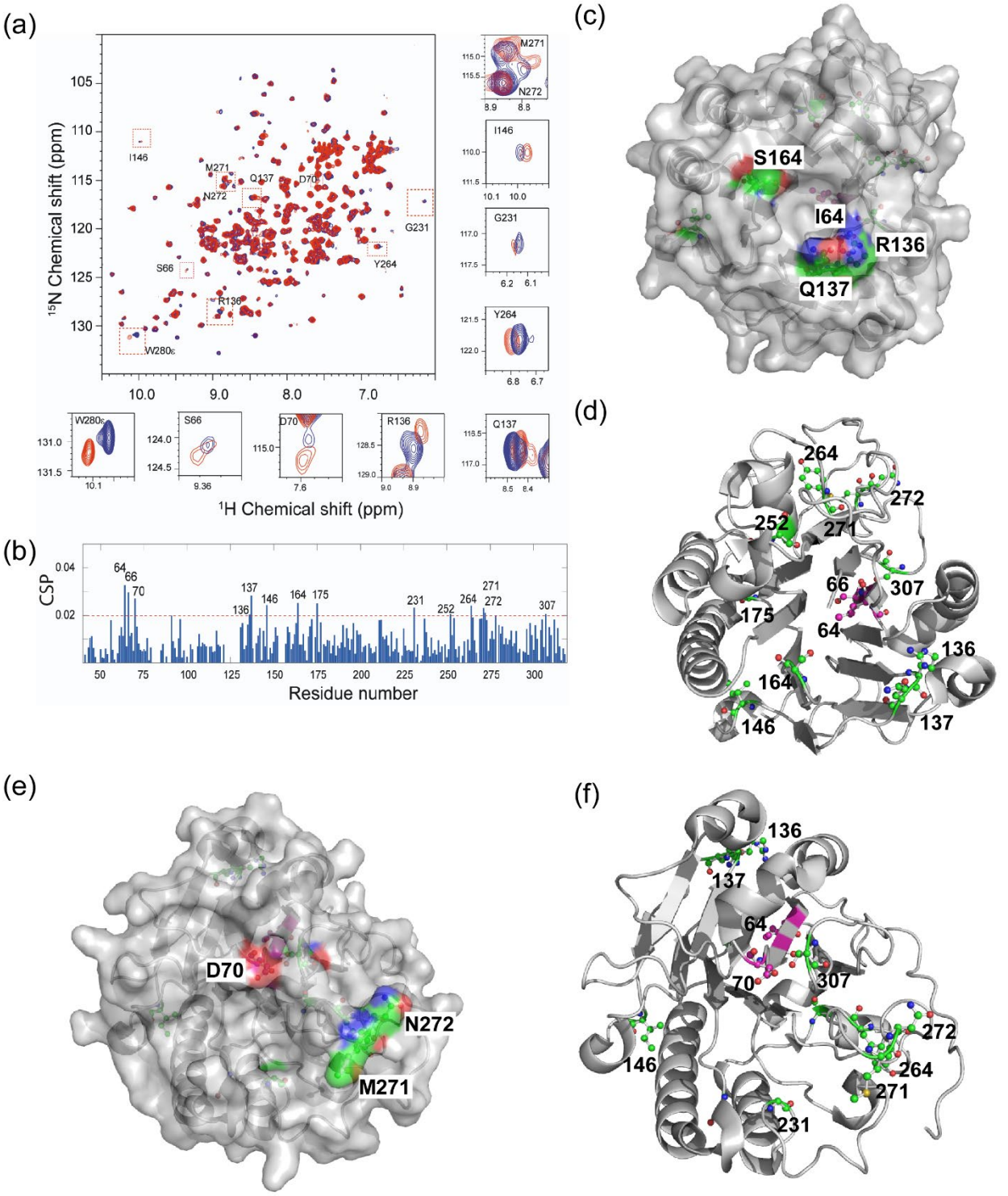

Fig. 3. Interaction of APX3330 results in widespread CSPs in APE1. (a) 2D ^{15}N-HSQC spectrum with the superimposition of the free protein spectrum (black) and spectra with APX33330 concentration 850 μM red. Each ^{1}H/^{15}N peak corresponds to one backbone or side chain amide. Specific chemical shift perturbations are shown in small boxes. (b) The chemical shift perturbations vs residue number reveal widespread interactions with APE1. Residues with CSPs

greater than 0.02 are shown as stick renderings (C, green, N, blue, O, red, or C magenta, for residues 64, 66, and 70) in semi-transparent gray surface rendering of APE1 (4QHD) in (c) and cartoon rendering in (d). Surface residues appear in color on the surface. In (c), a small pocket is defined by interactions with APX3330. In (d), buried residues with significant CSPs are evident. A view of APE1 rotated by approximately 180° is shown as a semi-transparent surface rendering in (e) and cartoon rendering in (f). A subset of surface residues (70, 271, and 272) with significant CSPs border the endonuclease active site, the large pocket shown in (e).

To map protons within APX3330 that are affected by interaction with APE1, we performed a 1D waterLOGSY experiment. This method effectively maps changes in solvent accessibility upon magnetization transfer from bulk water, waters bound to the protein, or waters trapped in a protein-ligand interface.[29-31] In this analysis, methylene 5 and methyl 6 protons within the nonyl hydrophobic tail, methyl protons 4 on the quinone ring, and the olefinic proton 1 (Fig. 1) exhibit peaks in the waterLOGSY difference spectrum (SI Fig. S6) suggesting that binding involves the hydrophobic tail of APX3330.

The small pocket defined by residues 136, 137, and 164 is the site of binding for a small molecule, 5-nitroindole-2-carboxylic acid, which is related to the reported APE1 inhibitor, 7-nitroindole-2-carboxylic acid (CRT0044876),[32] and identified in crystallographic and NMR studies,[33] although neither compound inhibited endonuclease activity of APE1 in this study. Attempts to model the binding of APX3330 in the small pocket were performed with molecular docking. Using both CDOCKER and AutoDock Vina programs,[34-35] a consensus pose for APX3330 was identified (Fig. 4). In this pose, the nonyl tail of APX3330 extends into the pocket to sit atop Leu62 and Ile91, while the methoxy and carbonyl oxygens of the benzoquinone ring form hydrogen bonds to Arg136 and Gln137. When aligned with the crystal structure of CRT0044876,[19] many atoms in APX3330 overlap well with atoms in the indole ring of CRT0044876, and the carboxylic acid group in APX3330 sits near a water molecule in the crystal structure and within hydrogen bonding distance of Thr61. In this manner, APX3330

contacts residues 136 and 137 that display high CSPs, as well as potential contacts to β-strands that comprise parts of the N- and C-termini of APE1, respectively.

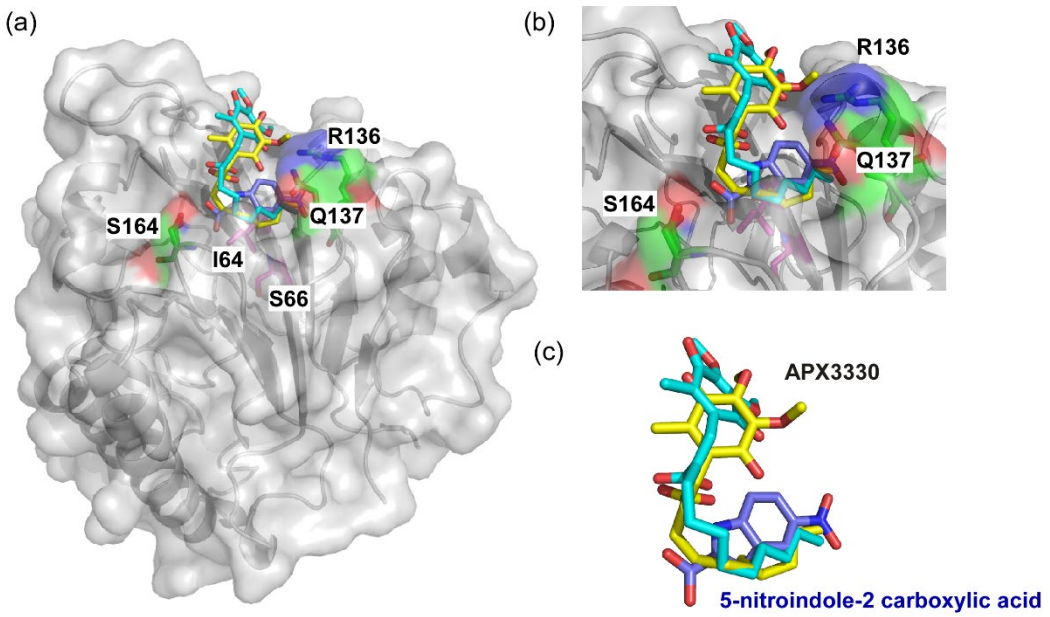

Figure 4. Docking of APX3330 based on crystal structure of CRT0044876 (7TC2). (a) A semi-transparent surface of APE1 (4QHD) is shown with residues R136, Q137, and S164 (stick model with C, green, O red, and N blue), which define the small pocket identified in the crystal structure and our CSP analysis. For reference, I64 and S66 are shown as stick models with C atoms in magenta. Consensus poses for APX3330 obtained from AutoDock Vina in yellow and CDOCKER in cyan are shown superimposed on the pose for CRT0004876 from the crystal structure. (b) A closeup view of the consensus poses shown in (a). (c) The consensus APX3330 models shown in yellow and cyan as indicated in (a) with CRT0044876 in blue.

In a previous NMR study examining the interactions of APX3330 with APE1, residues with significant CSPs included residues Gly231, Met270, Met271, Asn272, Ala273, Val278, Trp280, and Asp308, which are all located in the vicinity of the endonuclease active site.[23] Of note, residues 270-273 reside within a loop bordering the active site, with 271 and 272 in common in both studies. In that previous study, separate APE1 samples were prepared for each concentration of APX3330 used, in contrast to our study in which a titration was performed for a single APE1 sample.

Effects of APX3330 on APE1 partial denaturation are time dependent

Acquisition of the HSQC spectra for the APX3330 titration of APE1 (approximately 2-3 hours per spectrum) necessarily imposes time *and* concentration effects in the experiment. To investigate the time component, we incubated APE1 with an 8-fold molar excess of APX3330 as an intermediate concentration between 6-fold, which had few CSPs, and 10-fold molar excess, which had significantly more CSPs, and performed the study at 30 °C to accelerate the effects (Fig. 5). In this experiment, we observed a clear loss of backbone resonances after incubation longer than 20 hours.

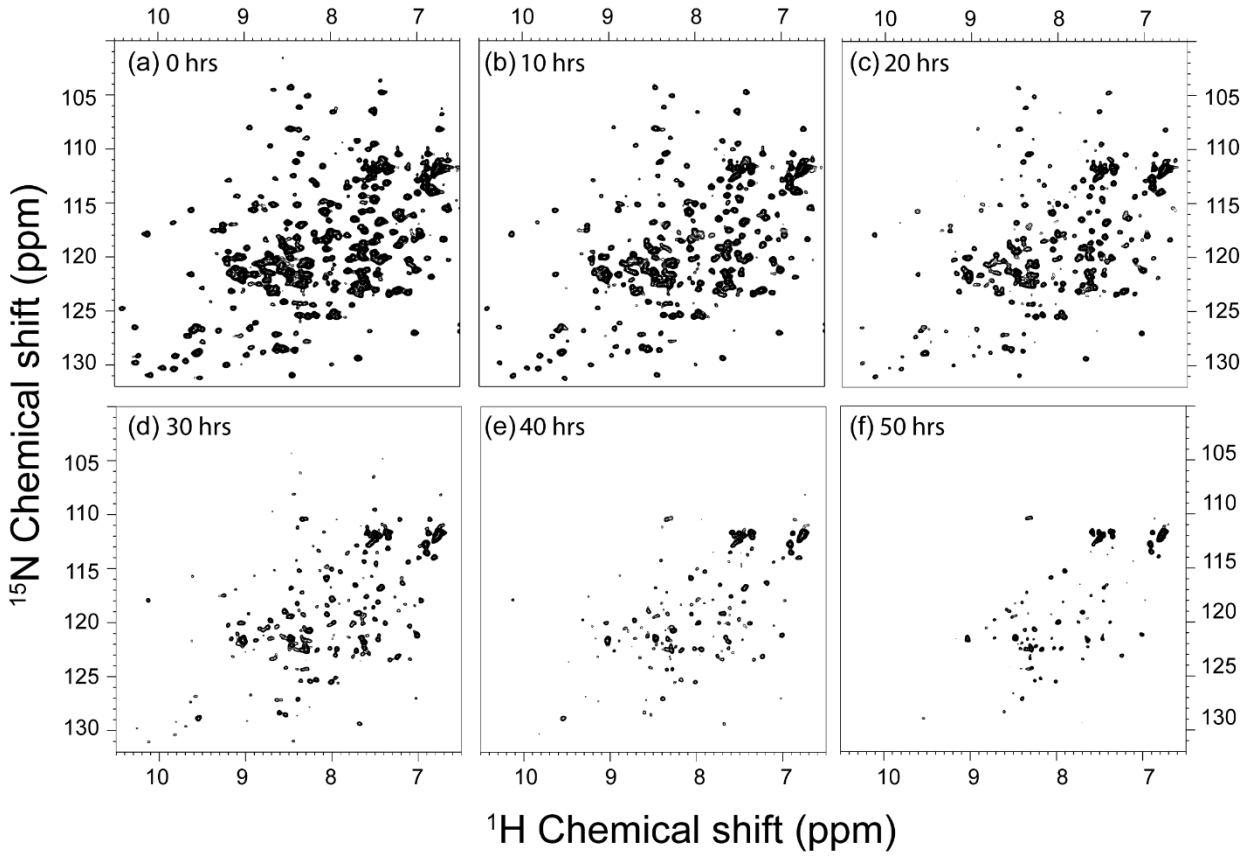

Fig. 5. Time dependent effects of APX3330 on [*U*-^{15}N]-APE1. HSQC spectra were collected at 30 °C for APE1 at (a) 0 hours following addition of an 8-fold molar excess of APX3330 (b) 10 hrs (c) 20 hrs (d) 30 hrs (e) 40 hrs and (f) 50 hrs. The peak intensities decrease as time progresses and approximately 35% of the backbone resonances are lost after 40 hrs; this spectrum appears similar to that of the 12-fold APX3330.

Assignment of the resonances remaining in the spectrum for the 40 h time point revealed a loss of 81 backbone resonances (~35% of the assigned resonances). These residues were mapped on the structure of APE1 along with regions that were not assigned in the native spectrum (Fig. 6a, b). APE1 has a core beta sandwich structure comprising a six-stranded beta sheet (sheet 1) and a five-stranded beta sheet (sheet 2). The N-terminal residues (39-62), which lack secondary structure, lead to a beta strand including residues 62-68 (strand 1) located within sheet 1 (Fig. 6c, d). The C-terminal region of the protein comprises strand 6 (residues 312-316), which is adjacent to strand 1 arising from the N-terminal region of the protein. Backbone resonances lost upon treatment with APX3330 include most of the residues within strands 1 (63-68) and 6 (312-314) along with residues in adjacent strands 2 (92-93) and 5 (299-301) all within sheet 1. Other secondary structural elements for which backbone resonances were lost include alpha helices 2, 4, 5, and 6. Among these, alpha helix 2 also lacks backbone resonance assignments for much of the helix. The remaining residues for which backbone resonances were lost in a time-dependent manner reside within loops.

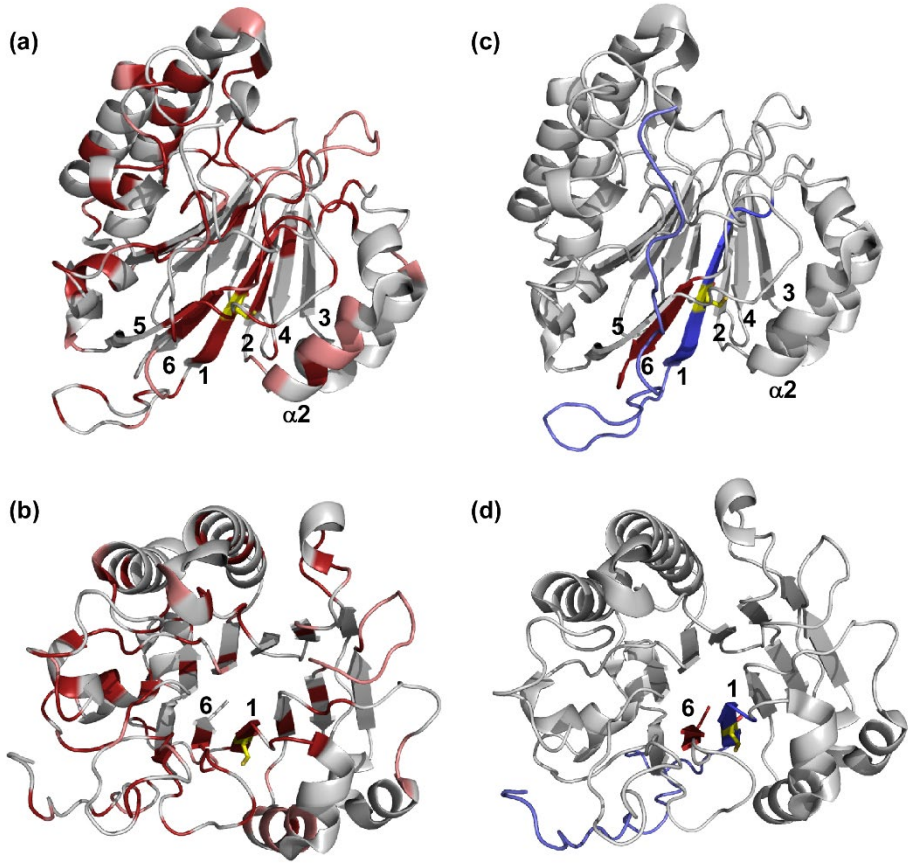

Fig. 6. Time-dependent effects of APX3330 on APE1. (a) Highlighted in red on a cartoon rendering of APE1 (4QHD) are the residues for which backbone resonances were lost in the 40 h time point in the HSQC spectrum, while in salmon are the residues that were initially unassigned. C65 located in strand 1 is shown as a yellow stick model. (b) A view of APE1 with the same residues highlighted looking down the beta sandwich. Numbering is shown for the strands comprising sheet 1 of the beta sandwich core. In (c) and (d), the same views of APE1 are shown with the N-terminal region highlighted in blue including strand 1 and the C-terminal region in red, including strand 6, highlighting the juxtaposition of the N- and C-terminal regions of the protein within sheet 1.

Consistent with the NMR experiments, treatment of APE1 with APX3330 revealed a time-dependent loss of secondary structure in CD experiments. Far-UV spectra for (260-190 nm) were measured at 25 and 30 °C. Prominent features include negative bands at 210 nm and 230 nm. The spectra for untreated APE1 are stable up to 5 days at 25 °C and 3 days at 30 °C, while treatment with APX3330 results in a loss in the intensity and a shift in the negative band at 210 nm and complete loss of the negative band at 230 nm (SI Fig. S7). These results are consistent

with the time-dependent loss of backbone resonances for some residues found in secondary structural element in the NMR experiments (Fig. 6).

Partial unfolding of APE1 by APX3330 is reversible in the presence of DNA

Having established that treatment with APX3330 impacts the folding of APE1, we next addressed the issue of reversibility using several different approaches. The first was to determine whether removal of excess APX3330 would be sufficient to restore fully folded APE1 as assessed by the ^{1}H-^{15}N HSQC spectrum. Removal of APX3330 by dialysis had no effect on the HSQC spectrum (SI Fig. S8). No loss of APE1 was evident following dialysis as measured by UV; however, loss of color in the sample suggested that excess APX3330 was removed. APX3330 in powder form is bright orange; samples including an 8-fold molar excess are yellow orange in color.

The next approach was to determine whether addition of duplex DNA substrate mimic (15-mer duplex containing a tetrahydrofuran mimic of an abasic site) would result in fully folded APE1. We first established the effect of adding duplex DNA to APE1. While addition of DNA clearly produced significant changes, the ^{1}H-^{15}N HSQC spectrum was well-resolved and consistent with folded APE1 as expected based on crystallographic studies of APE1 bound to DNA[28] (SI Fig. S9). APE1 bound to DNA shows significant chemical shift perturbations in ^{1}H-^{15}N HSQC spectrum. In 1D NMR spectra, the imino resonances of the DNA duplex containing the target site exhibit large changes in the chemical shifts on specific binding of the APE1 (SI Fig. S9). These differences are not only visible in the imino resonances but also in the aliphatic spectra regions. In the APE1 complex with substrate DNA containing a tetrahydrofuran abasic site mimic,[36] Arg177 and Met270 intercalate within the DNA stabilizing a bent conformation.

The aliphatic region clearly shows upfield shifts of the methyl resonances at the DNA protein binding site (SI Fig. S9).

Following treatment with APX3330 for two days, which resulted in partially unfolded APE1, duplex DNA was added to the sample; this produced some changes in the [1H-15N] HSQC spectrum of APE1 but clearly did not result in full folding of APE1 (Fig.7a). We then dialyzed the sample now containing partially unfolded APE1, APX3330, and DNA to remove excess APX3330 (as indicated by color loss) and obtained a well-resolved ^{1}H-^{15}N HSQC spectrum. We estimate that at least 40% of APE1 is fully folded in this sample (Fig. 7b).

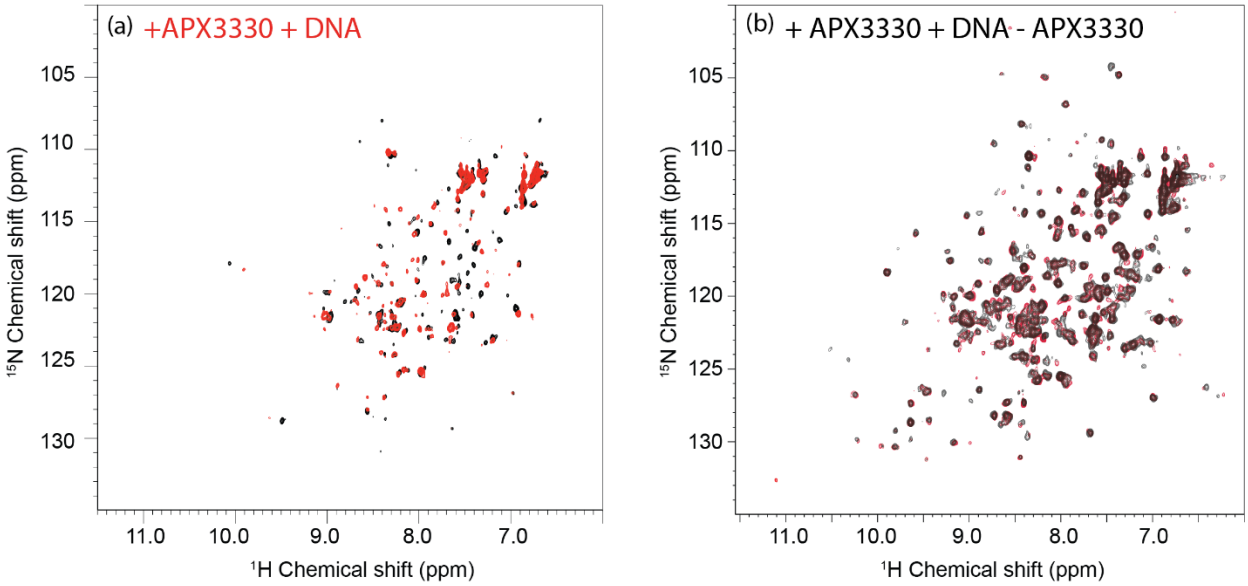

Fig. 7. Chemically induced partial unfolding of APE1 is reversible in the presence of DNA following removal of excess APX3330. (a) Following a 2 day incubation with APX3330 at an 8-fold molar excess, the ^{1}H-^{15}N HSQC spectrum of [*U*-^{15}N]-APE1 (black), DNA substrate mimic was added at a stochiometry of 1:1 (DNA:protein) (red); APE1 clearly did not refold. (b) The ^{1}H-^{15}N HSQC spectrum of [*U*-^{15}N]-APE1 treated with E3330, followed by addition of DNA, and then dialysis to remove excess APX3330 is shown in black. For comparison, the HSQC spectrum of APE1-DNA (1:1) complex is shown in red. The comparison illustrates that under the conditions of the experiment, APE1 has refolded.

APX3330 mechanism of action

A time-dependent effect was identified first in the APX3330 titration experiments, which were completed over a 24 h period. This phenomenon was then confirmed by treating APE1 with an 8-fold molar excess of APX3330 and monitoring the effects over time. Effectively, the 10-fold molar excess represents an early time point detailing the effects of APX3330 on APE1, albeit at a higher concentration. Taken together, the CSPs and time-dependent loss of backbone resonances suggest an unusual mechanism of action for the interaction of APX3330 with APE1. Residues 64 and 66 (within strand 1) show significant CSPs and the entire strand (consisting of residues 63-68) exhibits loss of backbone resonances. This strand is the most N-terminal secondary structural element in the APE1 fold. This finding, combined with loss of backbone resonances for the C-terminal residues 312-214 in the adjacent strand 6 of the sheet, suggests a mechanism in which APX3330 contributes to partial unfolding of APE1 through interactions with the N- and C-terminal strands in the sheet. Further, this process is likely facilitated by interactions with the small pocket defined by CSPs (Figs. 3 and 5).

We suggest that although initial binding likely involves a single APX3330 molecule binding to the small pocket as shown in Fig. 4, over time APX3330 forms, in essence, a reverse micelle involving interactions of the long alkyl chain by binding to the interior of the beta sandwich core, probably in a non-specific manner (i.e. rather than coating the outside of APE1, APX3330 coats the inside of the protein) resulting in the significant CSPs of internal residues, and the time-dependent loss of chemical shifts associated with strands in sheet 1. The effect cannot be reversed simply by removing excess APX3330, suggesting that the partially folded molecule is stabilized to some extent even in the absence of excess APX3330. The effect is reversible in the presence of a DNA substrate mimic as demonstrated by restoration of a well-

resolved HSQC spectrum following removal of excess APX3330. This finding is consistent with the more favorable state being the fully folded state that binds DNA.

Implications for APE1 function and future drug development

Although APE1 remains fully folded and stable for at least 20 days in a phosphate buffered solution, in the presence of excess APX3330, over time it begins to unfold. This unfolding involves the N-terminal strand 1 of sheet 1, which includes Cys65 and the C-terminal strand 6, which includes part of the mitochondrial targeting sequence (MTS) including residues 298-318. Alpha helix 2 adjacent to strand 1, which would normally shield Cys65, is also unfolded, as is adjacent strand 2. In the folded state, Cys65 is protected from oxidation. Partial unfolding would expose Cys65 potentially resulting in increased intermolecular disulfide bond formation with the most prevalent being between Cys65 and Cys93 in two APE1 molecules as previously reported,[37] which would affect its role as a redox factor and its role in mitochondrial trafficking.[18] As is the case for treatment of cells with hydrogen peroxide or menadione,[6] treatment with APX3330 results in relocalization of APE1 from the nucleus to the cytoplasm.[18] Further, there is no doubt that APE1 must unfold to expose the MTS and be transported to the inner mitochondrial space.[6] The presence of APX3330 bound to a partially unfolded state of APE1 may prevent interactions with mitochondrial transport proteins, Tom20,[6] or other cytoplasmic or mitochondrial chaperones such as Mia40.[38]

While APX3330 is currently in Phase II clinical trials, it continues to serve as a useful chemical tool in probing functional properties of APE1. In this study, it has allowed us to identify a possible mechanism of partial unfolding, it may yet inform future drug development. Specifically, targeting of the small pocket defined by residues 136, 137 and 164 and subsequent stabilization of a partially unfolded state of APE1 may affect mitochondrial trafficking, which

under conditions of oxidative stress may impact survival of dividing cells. APE1 is thought to repair damaged mitochondrial DNA during oxidative stress[5] in addition to degrading damaged mitochondrial mRNA.[39] While it is likely that the properties of APX3330 depend on the presence of a long alkyl chain, further modifications of this small molecule may yet produce even better inhibitors.

Methods

Protein expression and purification. APE1 (39-318/C138A) was expressed in *E. coli* and purified as previously described.[28] ^{15}N-APE1 (39-318/C138A) was expressed as a His-SUMO-fusion in BL21/Rosetta *E. coli*. 2L minimal media cultures were grown with ^{15}N-ammonium chloride as the sole nitrogen source.[40-41] Cells were grown at 37 °C until the culture reached an OD of 0.6; the cultures were then induced with 0.2 mM IPTG and grown for 4 hours at 37 °C. Cells were pelleted and stored at -80 °C prior to purification.

Cells were resuspended in 50 mM sodium phosphate, 0.3 M sodium chloride, 20 mM imidiazole pH 7.8 and lysed using a microfluidizer M110L. Following centrifugation at 35,000 rpm for 30 minutes, the supernatant was filtered and loaded on two 0.5 ml Ni-NTA (Qiagen) columns (one column/L growth) run at 4 °C. The column was washed with 10 column volumes of buffer and incubated with Ulp1 protease (10 μg/column) in 8 ml per column overnight. The flowthrough was then collected the next day. Labeled and unlabeled APE1 were assessed by SDS-PAGE and by QToF intact mass spectrometric analysis to confirm purity and mass.

NMR spectroscopy. 2D ^{1}H/^{15}N heteronuclear single-quantum coherence (HSQC) spectra were acquired at 25 °C or as indicated on a 600 MHz Bruker AVANCE spectrometer equipped with a 5-mm triple-resonance cryoprobe (^{1}H,^{13}C, and ^{15}N) and z-axis pulsed gradient. All NMR

experiments were processed using TOPSPIN and analyzed with CCPN NMR.[42] ^{15}N-labelled APE1 at a concentration of 80 μM was dialyzed against 20 mM sodium phosphate (pH 6.5), 0.1 M sodium chloride in 90%/10% H_2O/D_2O and placed in an NMR tube. The inhibitor APX3330 obtained from Apexian Pharmaceuticals was dissolved in acetonitrile-D3. For the inhibitor experiments, acetonitrile-D3 never exceeded 2% (v/v). The chemical shift perturbations (CSP) ($\Delta\delta$) were calculated using eq. 1, which reflects the total weighted change in ^{1}H and ^{15}N chemical shift for a given peak in the 2D spectra:

$$\Delta\delta = [(\Delta\delta H)^2 + (0.1\Delta\delta N)^2]^{1/2}$$

DNA oligonucleotides 5'-GCGTCCFCGACGACG (F indicates tetrahydrofuran serving as a mimic of an AP site) and 5'-CGTCGTCGAGGACGC were purchased from Integrated DNA Technologies, Inc., annealed, and used without further purification. DNA duplex was added to a final concentration of 80 μM to form a 1:05 (protein:DNA) complex with the protein along with 1 mM calcium chloride. While APE1 still cleaves DNA in the presence of calcium chloride, it does so much more slowly than with the preferred metal, magnesium.[43]

WaterLOGSY experiments were conducted at 303K in 5 mm diameter NMR tubes with a sample volume of 500 μL. APX3330 was prepared as 50 mM stock solutions in CD_3CN. Solutions were buffered in 20 mM sodium phosphate, 0.1 M NaCl pH 6.5 with 90% H_2O and 10% D_2O. WaterLOGSY experiments were done with 20 μM APE1 (39-318/C138A) and 200 μM compound for each experiment. The mixing time was set to 1.5 s and data were collected with 128 scans, a sweep width of 10 ppm, an acquisition time of 1.58 s, and a relaxation delay 5

seconds. Prior to Fourier transformation, the data were multiplied with an exponential function with a line broadening of 1 Hz.

Modeling of APX3330 interactions with APE1. Structural modeling of APX3330 bound to APE1 in a small binding site near residues 136, 137, and 164 was performed with rigid-receptor docking using AutoDock Vina (ADV) and the CHARMM-based CDOCKER docking algorithm.[34-35] Prior to docking, the apo structure of APE1 was taken from PDBID: 4QHD[28] and prepared with the MolProbity webserver[44-45] and PROPKA[46] to check for residue flips and determine appropriate protonation states for titratable residues at pH = 7.0. Receptor pdb coordinates were then formatted as a pdbqt file for ADV with the AutoDock Tools program;[47] pdb coordinates for CDOCKER were alternatively formatted with the CHARMM-GUI[48] and energy minimized with 200 steps of steepest decent minimization and the CHARMM36 protein force field.[49-50] APX3330 was then constructed using UCSF Chimera,[51] and subsequently formatted for ADV with AutoDock Tools or for CDOCKER via parameterization with the CHARMM Generalized Force Field (CGenFF).[52-54] Docking was performed in ADV using default settings and a cubic grid of 20 Å/edge centered on the binding site; however, 20 binding modes were generated using an exhaustiveness setting of 100, to account for the many degrees of freedom that could be sampled in the nonyl alkyl tail of APX3330. Similarly, default procedures were followed in CDOCKER,[34, 55] which uses a combination of grid-based simulated annealing molecular dynamics and all-atom energy minimization for pose identification and scoring, respectively. A total of 2000 poses were generated with CDOCKER. Manual inspection of the top 10 rank ordered docking poses from both ADV and CDOCKER was preformed to identify the lowest energy consensus structure for APX3330 bound to APE1. Figures were created with PyMOL.[56]

Circular dichroism experiments. Unlabeled APE1 (39-318) was used for CD experiments. The time dependence of APX3330 on APE1 secondary structure was evaluated by CD. Reactions included 80 μM APE1 (39-318) diluted from a 3 mM stock with either 1.3 % acetonitrile or 640 μM APX3330 (50 mM stock in acetonitrile) buffered in 20 mM sodium phosphate, 0.1 M NaCl pH 6.5 and incubated at either 25 ° or 30 °C. These are the conditions used for the time-dependent NMR experiments. Aliquots were removed from the reactions for CD measurements and diluted to give final concentrations of 20 μM APE1 and 120 μM APX3330. Controls showed that 1.3% acetonitrile had no effect on the CD spectrum of APE1. Data were measured on a Jasco J-1500 circular dichroism instrument with a Peltier temperature control device.

Acknowledgements

We acknowledge the Chemical Genomics Core Facility at IU School of Medicine which houses the 600 MHz NMR instrument and supports operational costs. J.Z.V. acknowledges the Indiana University Pervasive Technology Institute for providing supercomputing and storage resources that have contributed to the research results reported within this paper. This work was supported by NIH grants R01 CA231267 and R01CA167291 (M.R.K.), R01CA254110 (M.R.K. and M.M.G.) and P30CA082709 (IU Simon Comprehensive Cancer Center).

References

1. Kaur, G.; Cholia, R. P.; Mantha, A. K.; Kumar, R., DNA repair and redox activities and inhibitors of apurinic/apyrimidinic endonuclease 1/redox effector factor 1 (APE1/Ref-1): a comparative analysis and their scope and limitations toward anticancer drug development. *J Med Chem* **2014,** *57* (24), 10241-56.
2. Laev, S. S.; Salakhutdinov, N. F.; Lavrik, O. I., Inhibitors of nuclease and redox activity of apurinic/apyrimidinic endonuclease 1/redox effector factor 1 (APE1/Ref-1). *Bioorg Med Chem* **2017,** *25* (9), 2531-2544.
3. Lindahl, T.; Nyberg, B., Rate of depurination of native deoxyribonucleic acid. *Biochemistry* **1972,** *11* (19), 3610-3618.
4. Demple, B.; Herman, T.; Chen, D. S., Cloning and expression of APE, the cDNA encoding the major human apurinic endonuclease: definition of a family of DNA repair enzymes. *Proc Natl Acad Sci U S A* **1991,** *88* (24), 11450-4.
5. Grishko, V. I.; Rachek, L. I.; Spitz, D. R.; Wilson, G. L.; LeDoux, S. P., Contribution of mitochondrial DNA repair to cell resistance from oxidative stress. *J Biol Chem* **2005,** *280* (10), 8901-5.
6. Li, M.; Zhong, Z.; Zhu, J.; Xiang, D.; Dai, N.; Cao, X.; Qing, Y.; Yang, Z.; Xie, J.; Li, Z.; Baugh, L.; Wang, G.; Wang, D., Identification and characterization of mitochondrial targeting sequence of human apurinic/apyrimidinic endonuclease 1. *J Biol Chem* **2010,** *285* (20), 14871-14881.
7. Jackson, E. B.; Theriot, C. A.; Chattopadhyay, R.; Mitra, S.; Izumi, T., Analysis of nuclear transport signals in the human apurinic/apyrimidinic endonuclease (APE1/Ref1). *Nucleic Acids Res* **2005,** *33* (10), 3303-12.
8. McNeill, D. R.; Whitaker, A. M.; Stark, W. J.; Illuzzi, J. L.; McKinnon, P. J.; Freudenthal, B. D.; Wilson, D. M., 3rd, Functions of the major abasic endonuclease (APE1) in cell viability and genotoxin resistance. *Mutagenesis* **2020,** *35* (1), 27-38.
9. Mijit, M.; Caston, R.; Gampala, S.; Fishel, M. L.; Fehrenbacher, J.; Kelley, M. R., APE1/Ref-1 - One Target with Multiple Indications: Emerging Aspects and New Directions. *J Cell Signal* **2021,** *2* (3), 151-161.
10. Caston, R. A.; Gampala, S.; Armstrong, L.; Messmann, R. A.; Fishel, M. L.; Kelley, M. R., The multifunctional APE1 DNA repair-redox signaling protein as a drug target in human disease. *Drug Discov Today* **2021,** *26* (1), 218-228.
11. Malfatti, M. C.; Antoniali, G.; Codrich, M.; Tell, G., Coping with RNA damage with a focus on APE1, a BER enzyme at the crossroad between DNA damage repair and RNA processing/decay. *DNA Repair (Amst)* **2021,** *104*, 103133.
12. Davletgildeeva, A. T.; Kuznetsova, A. A.; Fedorova, O. S.; Kuznetsov, N. A., Activity of Human Apurinic/Apyrimidinic Endonuclease APE1 Toward Damaged DNA and Native RNA With Non-canonical Structures. *Front Cell Dev Biol* **2020,** *8*, 590848.
13. Kelley, M. R.; Georgiadis, M. M.; Fishel, M. L., APE1/Ref-1 role in redox signaling: translational applications of targeting the redox function of the DNA repair/redox protein APE1/Ref-1. *Current molecular pharmacology* **2012,** *5* (1), 36-53.
14. Xanthoudakis, S.; Curran, T., Identification and characterization of Ref-1, a nuclear protein that facilitates AP-1 DNA-binding activity. *EMBO J* **1992,** *11* (2), 653-65.
15. Walker, L. J.; Robson, C. N.; Black, E.; Gillespie, D.; Hickson, I. D., Identification of residues in the human DNA repair enzyme HAP1 (Ref-1) that are essential for redox regulation of Jun DNA binding. *Mol Cell Biol* **1993,** *13* (9), 5370-6.
16. Georgiadis, M.; Luo, M.; Gaur, R.; Delaplane, S.; Li, X.; Kelley, M., Evolution of the redox function in mammalian apurinic/apyrimidinic endonuclease. *Mutat Res* **2008,** *643* (1-2), 54-63.

17. Heisel, C.; Yousif, J.; Mijiti, M.; Charizanis, K.; Brigell, M.; Corson, T. W.; Kelley, M. R., APE1/Ref-1 as a Novel Target for Retinal Diseases. *J Cell Signal* **2021,** *2* (2), 133-138.
18. Vascotto, C.; Bisetto, E.; Li, M.; Zeef, L. A.; D'Ambrosio, C.; Domenis, R.; Comelli, M.; Delneri, D.; Scaloni, A.; Altieri, F.; Mavelli, I.; Quadrifoglio, F.; Kelley, M. R.; Tell, G., Knock-in reconstitution studies reveal an unexpected role of Cys-65 in regulating APE1/Ref-1 subcellular trafficking and function. *Mol Biol Cell* **2011,** *22* (20), 3887-901.
19. Fishel, M. L.; He, Y.; Reed, A. M.; Chin-Sinex, H.; Hutchins, G. D.; Mendonca, M. S.; Kelley, M. R., Knockdown of the DNA repair and redox signaling protein Ape1/Ref-1 blocks ovarian cancer cell and tumor growth. *DNA Repair (Amst)* **2008,** *7* (2), 177-86.
20. Mijit, M.; Liu, S.; Sishtla, K.; Hartman, G. D.; Wan, J.; Corson, T. W.; Kelley, M. R., Identification of Novel Pathways Regulated by APE1/Ref-1 in Human Retinal Endothelial Cells. *Int J Mol Sci* **2023,** *24* (2).
21. Shimizu, N.; Sugimoto, K.; Tang, J.; Nishi, T.; Sato, I.; Hiramoto, M.; Aizawa, S.; Hatakeyama, M.; Ohba, R.; Hatori, H.; Yoshikawa, T.; Suzuki, F.; Oomori, A.; Tanaka, H.; Kawaguchi, H.; Watanabe, H.; Handa, H., High-performance affinity beads for identifying drug receptors. *Nat Biotechnol* **2000,** *18* (8), 877-81.
22. Hiramoto, M.; Shimizu, N.; Sugimoto, K.; Tang, J.; Kawakami, Y.; Ito, M.; Aizawa, S.; Tanaka, H.; Makino, I.; Handa, H., Nuclear targeted suppression of NF-kappa B activity by the novel quinone derivative E3330. *J Immunol* **1998,** *160* (2), 810-9.
23. Manvilla, B. A.; Wauchope, O.; Seley-Radtke, K. L.; Drohat, A. C., NMR studies reveal an unexpected binding site for a redox inhibitor of AP endonuclease 1. *Biochemistry* **2011,** *50* (48), 10540-9.
24. Luo, M.; Delaplane, S.; Jiang, A.; Reed, A.; He, Y.; Fishel, M.; Nyland II, R. L.; Borch, R. F.; Qiao, X.; Georgiadis, M. M.; Kelley, M. R., Role of the multifunctional DNA repair and redox signaling protein Ape1/Ref-1 in cancer and endothelial cells: Small molecule inhibition of Ape1's redox function. *Antioxid Redox Signal* **2008,** *10* (11), 1853-67.
25. Su, D. A.; Delaplane, S.; Luo, M. H.; Rempel, D. L.; Vu, B.; Kelley, M. R.; Gross, M. L.; Georgiadis, M. M., Interactions of Apurinic/Apyrimidinic Endonuclease with a Redox Inhibitor: Evidence for an Alternate Conformation of the Enzyme. *Biochemistry* **2011,** *50* (1), 82-92.
26. Zhang, J.; Luo, M.; Marasco, D.; Logsdon, D.; LaFavers, K. A.; Chen, Q.; Reed, A.; Kelley, M. R.; Gross, M. L.; Georgiadis, M. M., Inhibition of apurinic/apyrimidinic endonuclease I's redox activity revisited. *Biochemistry* **2013,** *52* (17), 2955-66.
27. Manvilla, B. A.; Varney, K. M.; Drohat, A. C., Chemical shift assignments for human apurinic/apyrimidinic endonuclease 1. *Biomol NMR Assign* **2010,** *4* (1), 5-8.
28. He, H.; Chen, Q.; Georgiadis, M. M., High-resolution crystal structures reveal plasticity in the metal binding site of apurinic/apyrimidinic endonuclease I. *Biochemistry* **2014,** *53* (41), 6520-9.
29. Raingeval, C.; Cala, O.; Brion, B.; Le Borgne, M.; Hubbard, R. E.; Krimm, I., 1D NMR WaterLOGSY as an efficient method for fragment-based lead discovery. *J Enzyme Inhib Med Chem* **2019,** *34* (1), 1218-1225.
30. Huang, R.; Leung, I. K. H., Protein-Small Molecule Interactions by WaterLOGSY. *Methods Enzymol* **2019,** *615*, 477-500.
31. Dalvit, C.; Pevarello, P.; Tato, M.; Veronesi, M.; Vulpetti, A.; Sundstrom, M., Identification of compounds with binding affinity to proteins via magnetization transfer from bulk water. *J Biomol NMR* **2000,** *18* (1), 65-8.
32. Madhusudan, S.; Smart, F.; Shrimpton, P.; Parsons, J. L.; Gardiner, L.; Houlbrook, S.; Talbot, D. C.; Hammonds, T.; Freemont, P. A.; Sternberg, M. J.; Dianov, G. L.; Hickson, I. D., Isolation of a small molecule inhibitor of DNA base excision repair. *Nucleic Acids Res* **2005,** *33* (15), 4711-24.
33. Pidugu, L. S.; Servius, H. W.; Sevdalis, S. E.; Cook, M. E.; Varney, K. M.; Pozharski, E.; Drohat, A. C., Characterizing inhibitors of human AP endonuclease 1. *PloS one* **2023,** *18* (1), e0280526.

34. Wu, G.; Robertson, D. H.; Brooks, C. L., 3rd; Vieth, M., Detailed analysis of grid-based molecular docking: A case study of CDOCKER-A CHARMm-based MD docking algorithm. *J Comput Chem* **2003,** *24* (13), 1549-62.
35. Trott, O.; Olson, A. J., AutoDock Vina: improving the speed and accuracy of docking with a new scoring function, efficient optimization, and multithreading. *J Comput Chem* **2010,** *31* (2), 455-61.
36. Mol, C. D.; Izumi, T.; Mitra, S.; Tainer, J. A., DNA-bound structure and mutants reveal abasic DNA binding by APE1 DNA repair and coordination. *Nature* **2000,** *403* (451-455).
37. Luo, M.; Zhang, J.; He, H.; Su, D.; Chen, Q.; Gross, M. L.; Kelley, M. R.; Georgiadis, M. M., Characterization of the redox activity and disulfide bond formation in apurinic/apyrimidinic endonuclease. *Biochemistry* **2011,** *51* (2), 695-705.
38. Barchiesi, A.; Wasilewski, M.; Chacinska, A.; Tell, G.; Vascotto, C., Mitochondrial translocation of APE1 relies on the MIA pathway. *Nucleic Acids Res* **2015,** *43* (11), 5451-64.
39. Barchiesi, A.; Bazzani, V.; Jabczynska, A.; Borowski, L. S.; Oeljeklaus, S.; Warscheid, B.; Chacinska, A.; Szczesny, R. J.; Vascotto, C., DNA Repair Protein APE1 Degrades Dysfunctional Abasic mRNA in Mitochondria Affecting Oxidative Phosphorylation. *J Mol Biol* **2021,** *433* (18), 167125.
40. Jansson, M.; Li, Y. C.; Jendeberg, L.; Anderson, S.; Montelione, G. T.; Nilsson, B., High-level production of uniformly (1)(5)N- and (1)(3)C-enriched fusion proteins in Escherichia coli. *J Biomol NMR* **1996,** *7* (2), 131-41.
41. Snyder, D. A.; Chen, Y.; Denissova, N. G.; Acton, T.; Aramini, J. M.; Ciano, M.; Karlin, R.; Liu, J.; Manor, P.; Rajan, P. A.; Rossi, P.; Swapna, G. V.; Xiao, R.; Rost, B.; Hunt, J.; Montelione, G. T., Comparisons of NMR spectral quality and success in crystallization demonstrate that NMR and X-ray crystallography are complementary methods for small protein structure determination. *J Am Chem Soc* **2005,** *127* (47), 16505-11.
42. Skinner, S. P.; Fogh, R. H.; Boucher, W.; Ragan, T. J.; Mureddu, L. G.; Vuister, G. W., CcpNmr AnalysisAssign: a flexible platform for integrated NMR analysis. *J Biomol NMR* **2016,** *66* (2), 111-124.
43. Lowry, D. F.; Hoyt, D. W.; Khazi, F. A.; Bagu, J.; Lindsey, A. G.; Wilson, D. M., 3rd, Investigation of the role of the histidine-aspartate pair in the human exonuclease III-like abasic endonuclease, Ape1. *J Mol Biol* **2003,** *329* (2), 311-22.
44. Davis, I. W.; Leaver-Fay, A.; Chen, V. B.; Block, J. N.; Kapral, G. J.; Wang, X.; Murray, L. W.; Arendall, W. B., 3rd; Snoeyink, J.; Richardson, J. S.; Richardson, D. C., MolProbity: all-atom contacts and structure validation for proteins and nucleic acids. *Nucleic Acids Res* **2007,** *35* (Web Server issue), W375-83.
45. Chen, V. B.; Arendall, W. B., 3rd; Headd, J. J.; Keedy, D. A.; Immormino, R. M.; Kapral, G. J.; Murray, L. W.; Richardson, J. S.; Richardson, D. C., MolProbity: all-atom structure validation for macromolecular crystallography. *Acta crystallographica. Section D, Biological crystallography* **2010,** *66* (Pt 1), 12-21.
46. Olsson, M. H.; Sondergaard, C. R.; Rostkowski, M.; Jensen, J. H., PROPKA3: Consistent Treatment of Internal and Surface Residues in Empirical pKa Predictions. *J Chem Theory Comput* **2011,** *7* (2), 525-37.
47. *MGLTools: AutoDockToos, version 1.5.6*, Molecular Graphics Laboratory: The Scripps Research Institute, CA, 1999-2011.
48. Jo, S.; Kim, T.; Iyer, V. G.; Im, W., CHARMM-GUI: a web-based graphical user interface for CHARMM. *J Comput Chem* **2008,** *29* (11), 1859-65.
49. Best, R. B.; Mittal, J.; Feig, M.; MacKerell, A. D., Jr., Inclusion of many-body effects in the additive CHARMM protein CMAP potential results in enhanced cooperativity of alpha-helix and beta-hairpin formation. *Biophys J* **2012,** *103* (5), 1045-51.
50. Best, R. B.; Zhu, X.; Shim, J.; Lopes, P. E.; Mittal, J.; Feig, M.; Mackerell, A. D., Jr., Optimization of the additive CHARMM all-atom protein force field targeting improved sampling of the backbone phi, psi and side-chain chi(1) and chi(2) dihedral angles. *J Chem Theory Comput* **2012,** *8* (9), 3257-3273.

51. Pettersen, E. F.; Goddard, T. D.; Huang, C. C.; Couch, G. S.; Greenblatt, D. M.; Meng, E. C.; Ferrin, T. E., UCSF Chimera--a visualization system for exploratory research and analysis. *J Comput Chem* **2004,** *25* (13), 1605-12.
52. Vanommeslaeghe, K.; MacKerell, A. D., Jr., Automation of the CHARMM General Force Field (CGenFF) I: bond perception and atom typing. *J Chem Inf Model* **2012,** *52* (12), 3144-54.
53. Vanommeslaeghe, K.; Raman, E. P.; MacKerell, A. D., Jr., Automation of the CHARMM General Force Field (CGenFF) II: assignment of bonded parameters and partial atomic charges. *J Chem Inf Model* **2012,** *52* (12), 3155-68.
54. Vanommeslaeghe, K.; Hatcher, E.; Acharya, C.; Kundu, S.; Zhong, S.; Shim, J.; Darian, E.; Guvench, O.; Lopes, P.; Vorobyov, I.; Mackerell, A. D., Jr., CHARMM general force field: A force field for drug-like molecules compatible with the CHARMM all-atom additive biological force fields. *J Comput Chem* **2010,** *31* (4), 671-90.
55. Ding, X.; Hayes, R. L.; Vilseck, J. Z.; Charles, M. K.; Brooks, C. L., 3rd, CDOCKER and lambda-dynamics for prospective prediction in D(3)R Grand Challenge 2. *J Comput Aided Mol Des* **2018,** *32* (1), 89-102.
56. *The PyMOL molecular Graphics System, version 2.5.2*, Schrodinger LLC: New York, New York.